Int. J. Electrochem. Sci., 7 **(2012)** 6202 - 6213

International Journal of
ELECTROCHEMICAL
SCIENCE
www.electrochemsci.org

Attapulgite Clay Combined with Tris(2,2'bipyridyl)ruthenium(II) for the Enhancement of the Electrogenerated Chemiluminescence Sensing

Bin Gu[1,2], *Hui Zhong*[1,2,*], *Li-li Zhang*[1], *Zhi-Peng Cheng*[1], *Yin-zhu Wang*[2], *Xiao-mo Li*[1], *Ji-ming Xu*[1], *Cheng Yao*[2]

[1] Jiangsu Key Laboratory for Chemistry of Low-Dimensional Materials, School of Chemistry & Chemical Engineering, Huaiyin Normal University, Huaian 223300, P. R. China
[2] College of Sciences, Nanjing University of Technology, Nanjing 210009, P. R. China
[*]E-mail: huizhong@hytc.edu.cn

Received: 26 May 2012 / *Accepted:* 12 June 2012 / *Published:* 1 July 2012

This paper reports on the application of attapulgite for the immobilization of tris(2,2'-bipyridyl)ruthenium(II) ($[Ru(bpy)_3]^{2+}$) to improve its electrochemiluminescence (ECL) sensing. The attapulgite clay is a kind of natural nanomaterial and belongs to a family of fibrous hydrous magnesium silicates. The immobilized $[Ru(bpy)_3]^{2+}$ displayed a pair of well-defined redox peaks with an electron-transfer rate constant of 9.27 s^{-1} and a fast ECL response to oxalate and tripropylamine (TPA) in 0.1 M pH 7.0 phosphate buffer. The immobilized $[Ru(bpy)_3]^{2+}$ could maintain its ECL behavior in response to the co-reactants oxalate and TPA with high sensitivity. The ECL intensity was found to be linearly related to the concentration of oxalate over the range from 1.2 to 1080 μM, and the detection limit was 0.4 μM (S/N = 3). The linear concentration range for TPA extended from 1 nM to 5.4 μM and the detection limit (S/N = 3) was 0.5 nM, which is two orders of magnitude lower than that obtained at a $\{clay/[Ru(bpy)_3]^{2+}\}_n$ multilayer film modified electrode. Our study demonstrated that the low-cost and natural attapulgite is superior to previous nanomaterial for the enhancement of ECL detection and may provide a better approach for the practical application of ECL determination.

Keywords: $[Ru(bpy)_3]^{2+}$, electrogenerated chemiluminescence, attapulgite, electron transfer

1. INTRODUCTION

Electrogenerated chemiluminescence (ECL), the production of light from electrochemically generated reagents, is an optical signal triggered by an electrochemical reaction [1, 2] and has been extensively exploited as an important and valuable detection method in analytical chemistry[3-6]. In

recent years, ruthenium(II) complex-based ECL has become a powerful analytical tool because of its high sensitivity and wide linear range [7] for numerous analytes, such as alkylamines [8], organic acids [9], NADH [10], amino acids [11], alkaloids [12], oxalates [13], and so on.

Compared with the solution-phase ECL procedure, the immobilization of $[Ru(bpy)_3]^{2+}$ on a solid electrode surface can provide several advantages, such as the reduction of the consumption of expensive reagent, the enhancement of the ECL signals, and the simplification of the experimental designs [14]. To date, various methods have been applied for the immobilization of $[Ru(bpy)_3]^{2+}$ with a view to developing a cost-effective and regenerable chemical sensor [15–18]. $[Ru(bpy)_3]^{2+}$ can be immobilized on an electrode surface as a monolayer by way of a Langmuir–Blodgett film [19, 20] or by a self-assembled monolayer [21, 22] with derivatives of $[Ru(bpy)_3]^{2+}$. However, these films have proved to be unstable under high applied potentials. The incorporation of $[Ru(bpy)_3]^{2+}$ within a cation-exchange polymer such as Nafion [23, 24] through electrostatic interaction is another popular method. However, Nafion film has drawbacks because of slow mass-transfer through the film and the partition of $[Ru(bpy)_3]^{2+}$ into the hydrophobic regions of Nafion [17, 23], although these problems have been ameliorated by the incorporation of silica nanocomposites [25–27] or sol–gel-derived titania [28]. The long-term stability of such films is still limited by the high hydrophobicity of Nafion. The immobilization of $[Ru(bpy)_3]^{2+}$ in Eastman AQ55D silica-composite thin films [29], silica sol–gels [30, 31], and a combination of sol–gels and polyHEMA membranes [18] has been reported for the preparation of electrochemiluminescent sensors for oxalate, tripropylamine, and chlorpromazine All of these approaches have been shown to be promising, but new inexpensive doped materials, as well as simple and facile immobilization approaches, are still necessary for the development of stable and efficient ECL sensors.

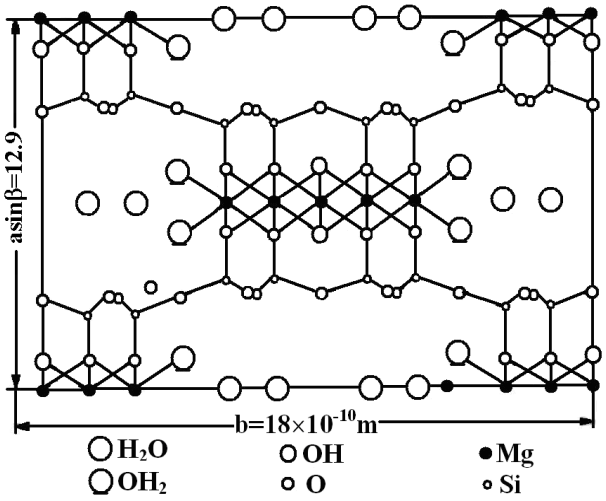

Figure 1. Crystalline structure of attapulgite from the (001) plane.

Attapulgite clay belongs to a family of fibrous hydrous magnesium silicates [32] characterized by a special laminated chain structure in which there is a crystalline lattice displacement. Its ideal molecular formula is $Mg_5Si_8O_{20}(HO)_2(OH_2)_4 \cdot 4H_2O$. The structure was first proposed by Bradley [33]

and is shown in Fig. 1. Its mineral structure consists of zeolite-like channels, the cross-sectional dimensions of which are approximately 3.7 Å × 6.0 Å and 5.6 Å × 11.0 Å, respectively [32], and these cross-sections may be occupied by water or other molecules. Attapulgite has permanent negative charges on its surface, and a larger surface area and a stronger absorptive capacity than any other natural minerals [34]. As a kind of clay, attapulgite appears to be particularly attractive as a host matrix for the development of reactors or sensors due to its low cost, high chemical stability, ion-exchange properties, and unique fibrous aluminosilicate structure, which can form well-ordered coatings of appreciable surface area on electrode surfaces [35, 36].

In this work, we made use of natural nanostructured attapulgite as a matrix for the immobilization of $[Ru(bpy)_3]^{2+}$ in the ECL detection. Our measurements demonstrated that $[Ru(bpy)_3]^{2+}$ cations can be effectively immobilized on the surface of an attapulgite-modified glassy carbon (GC) electrode. Our results demonstrated that the nanostructured attapulgite is effective in preventing the immobilized $[Ru(bpy)_3]^{2+}$ from leaching into the solution due to the strong electrostatic interaction between the negatively charged attapulgite surface and the positively charged $[Ru(bpy)_3]^{2+}$ cations. With our approach, the ECL detection of oxalate and TPA was also carried out with high sensitivity.

2. EXPERIMENTAL

2.1. Materials

Tris(2,2'-bipyridyl)dichlororuthenium(II) hexahydrate ($[Ru(bpy)_3Cl_2]\cdot 6H_2O$) and tripropylamine (TPA) were purchased from Aldrich and used as received. Sodium oxalate was obtained from Shanghai Chemical Reagent Factory and Shanghai Biotechnology Co. Ltd. (Shanghai). Attapulgite micropowder was supplied by Hongqing Attapulgite Co., Ltd. (Xuyi, Jiangsu, China). Prior to use, attapulgite micropowder (4 g) was dispersed in water (100 mL) with the aid of ultrasonication for 1 h, and then the suspension was centrifuged; this process was repeated three times. 0.1 M phosphate buffer solutions were prepared by mixing stock standard solutions of Na_2HPO_4 and KH_2PO_4 and adjusting the pH with 0.1 M H_3PO_4 and NaOH. All other reagents were of analytical grade, and doubly-distilled water was used throughout.

2.2. Apparatus

Transmission electron microscopy (TEM) observation of attapulgite was carried out with a JEM-200CX TEM instrument operating at an accelerating voltage of 200 kV. The sample for TEM characterization was prepared by dropping a solution containing attapulgite onto a carbon-coated copper grid and drying at room temperature.

Wide-angle X-ray spectra were recorded with an ARL/X/TRA X-ray diffractometer (Switzerland). The X-ray beam was nickel-filtered Cu-$K_{\square}$ (λ=0.154056 nm) radiation operated at 45kV and 40 mA. Data were collected from 3 to 60□ at a scanning rate of 1□/min.

Cyclic voltammetric experiments were performed with an Autolab PGSTAT30 (EcoChemie, Utrecht, The Netherlands). ECL signals were monitored with an MPI-M multifunctional chemiluminescent and bioluminescent analytical system (Remax Electronic Co. Ltd., Xi'an, China) with the voltage of the photomultiplier tube (PMT) set at 800 V. The working electrode was of $[Ru(bpy)_3]^{2+}$/attapulgite-modified glassy carbon (GC). An Ag/AgCl (satd. KCl) reference electrode was used for all measurements. A platinum wire was used as auxiliary electrode.

2.3. Preparation of the immobilized $[Ru(bpy)_3]^{2+}$/attapulgite-modified glassy carbon electrode

Before preparation of the $[Ru(bpy)_3]^{2+}$/attapulgite-modified electrode, a glassy carbon electrode (diameter 3.0 mm) was sequentially polished with 1, 0.3, and 0.05 μm α-Al_2O_3, subjected to ultrasonic treatment after each polish, and then dried at room temperature. 5 μL of 2.0 mg/mL attapulgite colloid solution was then spread onto the pre-treated GC electrode surface and allowed to dry for 1 h to obtain the attapulgite-modified glassy carbon electrode. The attapulgite-modified electrode was then immersed in a 1.0 mmol L^{-1} $[Ru(bpy)_3]^{2+}$ aqueous solution for 1 h to immobilize this cation on its surface. The electrode was then thoroughly washed with water, stored under ambient conditions, and employed as an ECL sensor.

3. RESULTS AND DISCUSSION

3.1. Morphology and UV/Vis spectrum of $[Ru(bpy)_3]^{2+}$/attapulgite

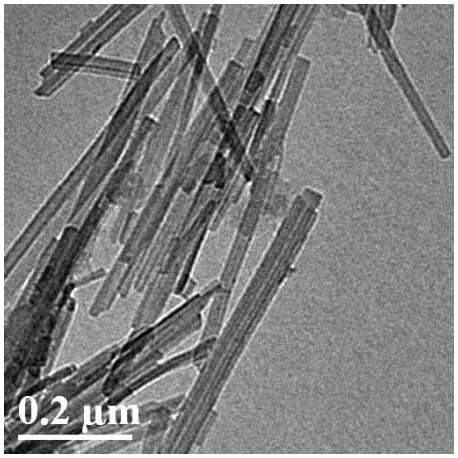

Figure 2. TEM image of attapulgite.

The morphology of attapulgite was characterized by TEM as shown in Fig. 2. It can be seen that the attapulgite has a fibrous morphology, made up of fibers of diameter 20–50 nm and length 300–1000 nm. The XRD pattern of attapulgite (see Fig. 3) showed diffraction peaks at 2θ=8.3, 13.6, 19.7, and 26.6°, which correspond to the primary diffractions of the (110), (200), (040), and (400) planes of the clay, respectively, and conform to the typical four-plane characteristic peaks of attapulgite.

Because of its unique structure, attapulgite seems to represent an ideal material for the immobilization of $[Ru(bpy)_3]^{2+}$ on a solid electrode surface.

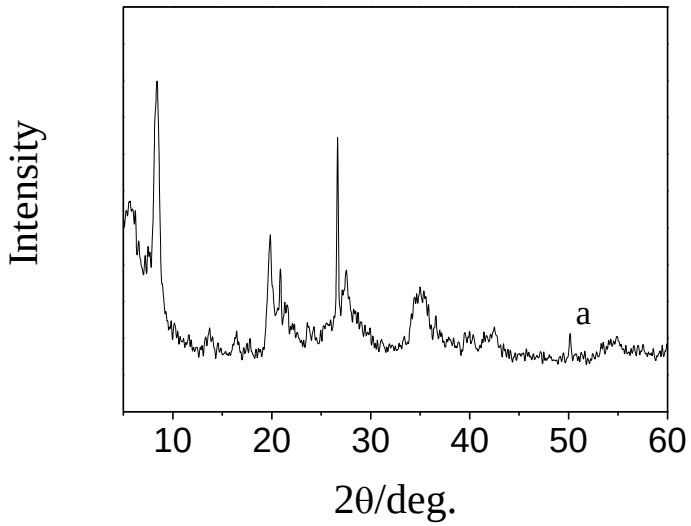

Figure 3. XRD pattern of attapulgite.

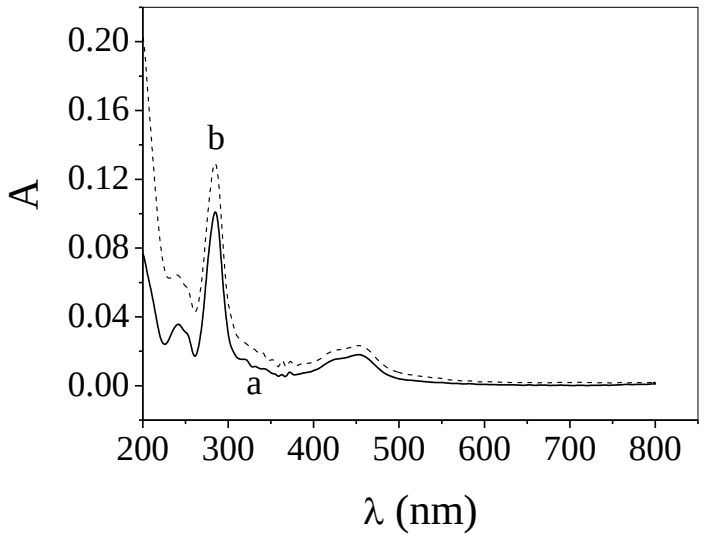

Figure 4. UV/Vis spectra of $[Ru(bpy)_3]^{2+}$/attapulgite (a) and $[Ru(bpy)_3]^{2+}$ (b).

The spectral properties of $[Ru(bpy)_3]^{2+}$/attapulgite were studied by UV/Vis spectroscopy. Fig. 4 shows the spectra of free $[Ru(bpy)_3]^{2+}$ and $[Ru(bpy)_3]^{2+}$/attapulgite on quartz slides. Two significant peaks at 287 and 454 nm were observed for free $[Ru(bpy)_3]^{2+}$, corresponding to a ligand-centered transition and metal-to-ligand transfer [37]. A similar pair of peaks (289 and 454 nm) were observed for the $[Ru(bpy)_3]^{2+}$/attapulgite. The appearance of two peaks at 289 and 454 nm demonstrated that $[Ru(bpy)_3]^{2+}$ incorporated into the attapulgite retained its optical properties. It also indicated that

$[Ru(bpy)_3]^{2+}$ cations had been successfully doped in the large cavities of attapulgite through ion exchange.

3.2. Electrochemistry of the $[Ru(bpy)_3]^{2+}$/attapulgite-modified electrode

The electrochemical behavior of the modified electrode made from $[Ru(bpy)_3]^{2+}$ immobilized in attapulgite clay was studied by means of cyclic voltammetry. Attapulgite is anionic, while $[Ru(bpy)_3]^{2+}$ is positively charged. Thus, $[Ru(bpy)_3]^{2+}$ can be readily incorporated into the cation-exchangeable attapulgite clay through electrostatic interactions.

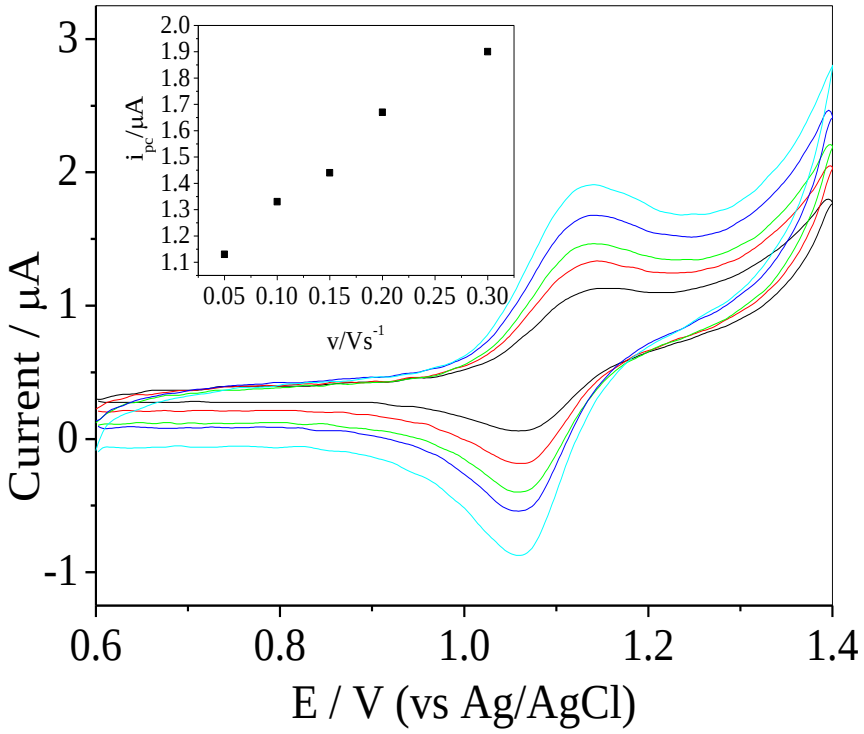

Figure 5. Cyclic voltammograms of $[Ru(bpy)_3]^{2+}$/attapulgite in 0.10 M pH 7.0 phosphate buffer at 0.05, 0.1, 0.2, 0.3, and 0.4 V s^{-1} (from lowest to highest peak currents). Inset: dependence of cathodic peak current on scan rate.

Fig. 5 shows cyclic voltammograms of the $[Ru(bpy)_3]^{2+}$/attapulgite-modified electrode at various scan rates. The cyclic voltammograms of the modified electrode show a redox couple at +1132 mV and +1074 mV, which may be attributed to the one-electron redox reaction of $[Ru(bpy)_3]^{2+}$. The potential difference between the oxidation and reduction peaks is 58 mV, which is an indicative of the good electrochemical reversibility of $[Ru(bpy)_3]^{2+}$ immobilized in attapulgite. Both the anodic and cathodic peak currents were increased linearly on increasing the scan rate from 20 to 500 mV s^{-1}. This revealed that the electrochemical reaction was a surface-confined process. From the peak-to-peak separations of the cyclic voltammograms of the immobilized $[Ru(bpy)_3]^{2+}$ obtained at different scan

rates, an average electron-transfer rate constant of 9.27 s^{-1} was obtained by using Laviron's model, and an electron-transfer number of 1 with an electron-transfer coefficient, α, of 0.35 was obtained from the slope of a plot of E_{pc} vs. v [38].

3.3. ECL behavior

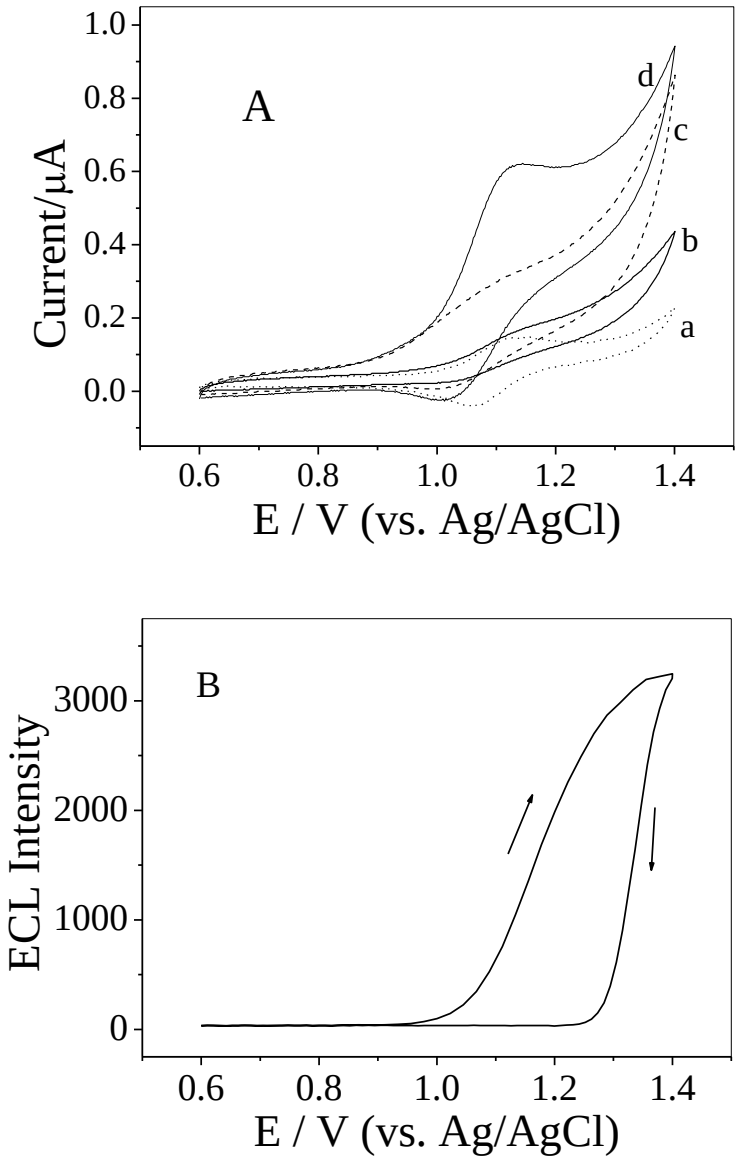

Figure 6. Cyclic voltammograms (A) of $[Ru(bpy)_3]^{2+}$/attapulgite- (a, d) and attapulgite-modified electrodes (c, b) in pH 7.0 phosphate buffer before (a, c) and after (b, d) addition of 0.4 μM $Na_2C_2O_4$ at 0.1 V s^{-1} and the corresponding ECL (B).

After the successful immobilization of $[Ru(bpy)_3]^{2+}$ in attapulgite, oxalate was chosen as the analyte for the investigation of the ECL behavior and its analytical application. Fig. 6 shows cyclic voltammograms of attapulgite- and $[Ru(bpy)_3]^{2+}$/attapulgite-modified GC electrodes in pH 7.0

phosphate buffer solution containing 0.4 mM $Na_2C_2O_4$ obtained at a scan rate of 100 mV s^{-1}. No redox peaks could be observed at the attapulgite-modified electrode in the range from 0.6 to 1.4 V (curve a and d in Fig. 6 A). However, under the same conditions, the $[Ru(bpy)_3]^{2+}$/attapulgite-modified GC electrode clearly showed a pair of peaks at +1132 mV and +1074 mV, indicating the electroactivity of the cations after they were entraped in attapulgite.

Upon addition of oxalate to pH 7.0 phosphate buffer, the anodic peak current of the cyclic voltammogram of the $[Ru(bpy)_3]^{2+}$/attapulgite-modified electrode showed a significant increase, while the cathodic current decreased (curves a and d in Fig. 6 A). The changes in the cathodic and anodic currents at the $[Ru(bpy)_3]^{2+}$/attapulgite-modified electrode were much larger than those at the attapulgite-modified electrode (curves c and b in Fig. 6 A), indicating the occurrence of a chemical reaction between oxalate and the oxidized form of $[Ru(bpy)_3]^{2+}$, $[Ru(bpy)_3]^{3+}$, which led to the electrogeneration of $[Ru(bpy)_3]^{2+}$ during the cyclic sweep [39].

At the same time, a corresponding ECL signal was observed in the anodic process (Fig. 6 B). The ECL intensity–potential curve displayed a steep increase around the anodic peak potential of the immobilized $[Ru(bpy)_3]^{2+}$. No ECL signal was observed before the potential reached the oxidation peak potential. With increasing pH, the ECL intensity increased and reached a maximum value at pH 7.0. At pH 7.0, the ECL intensity increased linearly with increasing $C_2O_4^{2-}$ concentration over the range from 1.2 to 1080 μM, with a correlation coefficient of 0.9969. From the slope of 0.0186 μmol L^{-1} and the signal-to-noise ratio of three, the detection limit was determined as 0.40 μM. This detection limit for $C_2O_4^{2-}$ is of the same order of magnitude as that obtained at a $\{clay/[Ru(bpy)_3]^{2+}\}_n$ multilayer-film modified electrode [40]. The relative standard deviation (RSD) for ten repeated determinations of ECL intensity at 100 μM $C_2O_4^{2-}$ was 2.1%.

We also investigated the ECL behavior of the $[Ru(bpy)_3]^{2+}$-immobilized attapulgite-modified electrode with TPA as an analyte, since the $[Ru(bpy)_3]^{2+}$–TPA system has been well characterized and shown to give rise to about tenfold higher ECL as compared to other commonly used co-reactants such as oxalate [41, 42].

When the deprotonated TPA radical (TPA*) is formed through reduction of $[Ru(bpy)_3]^{3+}$ or by direct electrode oxidation, the ECL emission of the $[Ru(bpy)_3]^{2+}$–TPA system arises. This system then reacts with another $[Ru(bpy)_3]^{2+}$ or additional $[Ru(bpy)_3]^{3+}$ to form $\{[Ru(bpy)_3]^{2+}\}^*$, which then begins to decay with the production of an orange emission. The simplified ECL reaction scheme may be summarized as follows [43,44]:

$$[Ru(bpy)_3]^{2+} \rightarrow [Ru(bpy)_3]^{3+} + e^- \quad (1)$$

$$[Ru(bpy)_3]^{3+} + TPA \rightarrow [Ru(bpy)_3]^{2+} + TPA^{+*} \quad (2a)$$

$$TPA \rightarrow TPA^{+*} + e^- \quad (2b)$$

$$TPA^{+*} \rightarrow TPA^{*} + H^+ \quad (3)$$

$$[Ru(bpy)_3]^{3+} + TPA^{*} \rightarrow \{[Ru(bpy)_3]^{2+}\}^{*} \quad (4)$$

$$\{[Ru(bpy)_3]^{2+}\}^{*} \rightarrow [Ru(bpy)_3]^{2+} + h\nu\ (610\ nm) \quad (5)$$

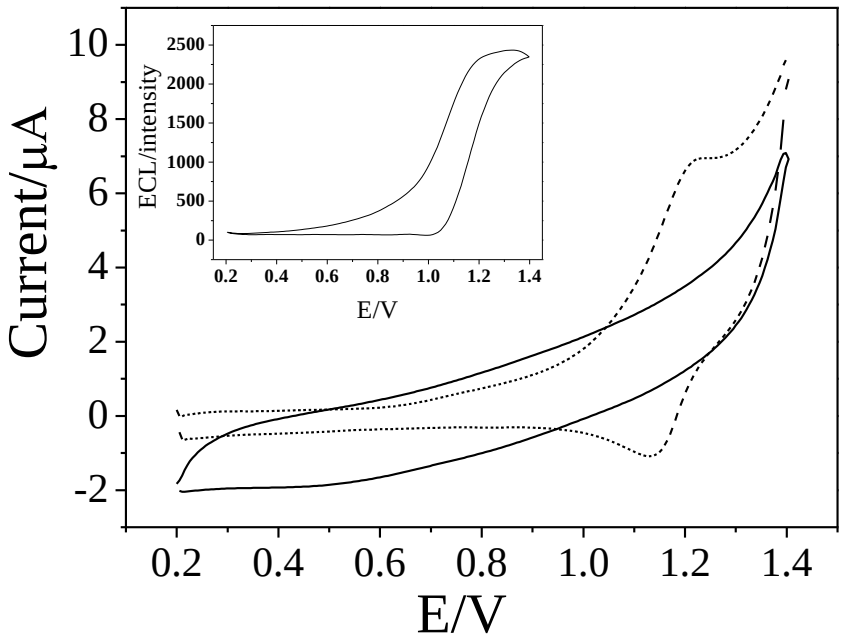

Figure 7. Cyclic voltammograms of $[Ru(bpy)_3]^{2+}$ immobilized on the attapulgite-modified electrode in the absence and presence of 1.0 μM TPA in 0.1 M phosphate buffer (pH 7.0) at a scan rate of 50 mV s^{-1}. Inset: The corresponding I_{ECL}–E curve of $[Ru(bpy)_3]^{2+}$ immobilized on the attapulgite-modified electrode in 1.0 μM TPA.

Fig. 7 shows the cyclic voltammograms of $[Ru(bpy)_3]^{2+}$ immobilized on the attapulgite-modified electrode in the presence (dashed line) or absence (solid line) of 1.0 μM TPA obtained at 50 mV s^{-1} in 0.1 M phosphate buffer (pH 7.0). The onset of luminescence occurs near 1.0 V, and then the ECL intensity rises steeply until it reaches the maximum value at around 1.25 V, which is consistent with the oxidation potential of $[Ru(bpy)_3]^{2+}$. The ECL signal intensified greatly in the presence of TPA because of the ECL reaction of $[Ru(bpy)_3]^{3+}$ with this base. The corresponding ECL intensity–potential profile is shown in the inset of Fig. 7. The ECL intensity was high, and the ECL response at the modified electrode was very fast because of the strong electrostatic interaction between the negatively charged attapulgite surface and the positively charged $[Ru(bpy)_3]^{2+}$ cations, which provides a favorable environment for the ECL reaction.

TPA has been shown to be the most efficient amine for the $[Ru(bpy)_3]^{2+}$ ECL reaction due to its structural attributes. To assess its sensitivity, the $[Ru(bpy)_3]^{2+}$-modified electrode has been used to determine TPA in our experiments. Fig. 8 shows a typical log–log calibration plot for TPA at attapulgite containing immobilized $[Ru(bpy)_3]^{2+}$. The height of the ECL peak was obtained from the ECL–potential curve acquired at 50 mV s^{-1} in phosphate buffer (pH 7.0). The linear concentration range extended from 1 nM to 5.4 μM (correlation coefficient: 0.996). The detection limit (S/N = 3) for TPA was estimated to be 0.5 nM, which is two and three orders of magnitude lower than those obtained at electrodes modified with $\{clay/[Ru(bpy)_3]^{2+}\}_n$ multilayer films [40] and Nafion–silica [26], respectively.

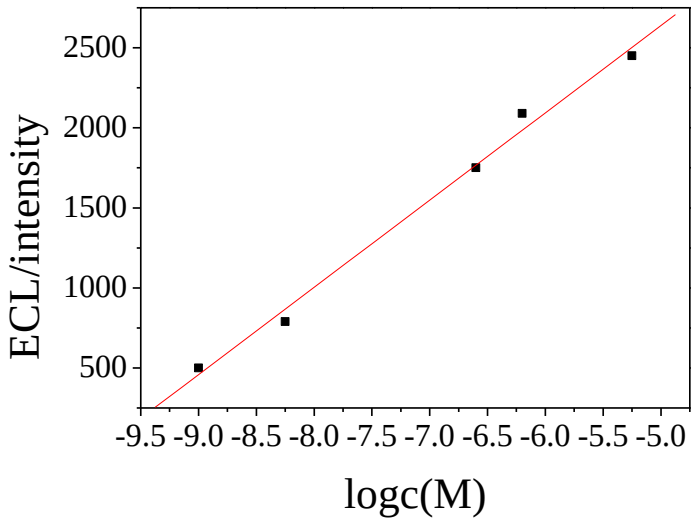

Figure 8. Calibration plot for TPA with $[Ru(bpy)_3]^{2+}$ immobilized in attapulgite.

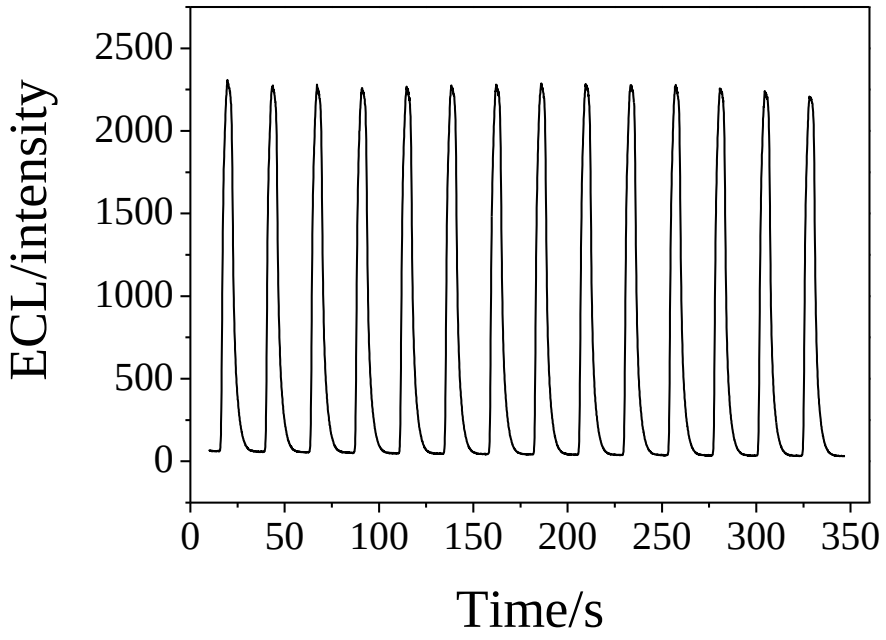

Figure 9. ECL emission from $[Ru(bpy)_3]^{2+}$ immobilized in attapulgite in phosphate buffer solution (pH 7.5) containing 1.0 μM TPA. Scan rate: 50 mV s^{-1}.

When the sensor was not in use, it was stored at room temperature. The long-term storage stability of the present ECL sensor based on the $[Ru(bpy)_3]^{2+}$/attapulgite-modified electrode was studied for over a month by monitoring its ECL response to 50 μM oxalate and 0.1 μM TPA in 0.1 M phosphate buffer solution (pH 7.0) by intermittent usage (at 2 or 3 day intervals). Moreover, Fig. 9 shows the ECL emission from $[Ru(bpy)_3]^{2+}$ immobilized in attapulgite in 1.0 μM TPA under continuous potential scanning for 14 cycles; it can be seen that there was no obvious decrease in the

ECL intensity. The results suggest that charge transfer in attapulgite be very fast and quite stable. Thus, the electrochemical stability of $[Ru(bpy)_3]^{2+}$ immobilized in attapulgite for use in the sensor was excellent. This good stability may be attributed to the natural nanostructure of attapulgite, which has permanent negative charges on its surface, a large surface area, and strong absorptive capacity.

4. CONCLUSIONS

The natural nanostructured attapulgite was successfully applied for the immobilization of $[Ru(bpy)_3]^{2+}$ on the glassy carbon electrode for the preparation of a ECL sensor. In electrochemistry, the immobilized $[Ru(bpy)_3]^{2+}$ displayed a surface-controlled quasi-reversible electrode process. Its analytical application was demonstrated by the ECL detection of oxalate and TPA. Considering the low cost of attapulgite clay, the fabricated ECL sensor is superior to other nanomaterials on the dramatic decrease of the amount of expensive $[Ru(bpy)_3]^{2+}$. This work provides a new approach for the immobilization of $[Ru(bpy)_3]^{2+}$ based on attapulgite in electrogenerated chemiluminescence.

ACKNOWLEDGEMENTS
This work was supported by National Natural Science Foundation of China (20975043, 51106061) and Jiangsu Province (BK2010289), Jiangsu Higher Institutions Key Basic Research Projects of Natural Science(09KJA530001, 10KJA430005), Qing Lan Project. All the authors here express their deep thanks.

References

1. N. E. Tokel, A. J. Bard, *J. Am. Chem. Soc*. 94 (1972) 2862.
2. B. A. Gorman, P. S. Francis, N. W. Barnett, *Analyst* 131 (2006) 616.
3. M.S Wu , B.Y. Xu , H.W. Shi , J.J. Xu and H.Y. Chen, *Lab Chip*, 11 (2011) 2720.
4. A Devadoss , Dickinson C, Keyes TE, *Forster RJ.Anal Chem.* 83 (2011) 2383.
5. K. N. Swanick , S. Ladouceur , Z.F. Ding *Chem. Commun*, 48 (2012) 3179.
6. Y. Zhang, S. Ge , S. Wang , M. Yan , J. Yu , X. Song , W. Liu *Analyst.* 137 (2012) 2176.
7. K. A. Fahnrich, M. Pravda, G. G. Guilbault, *Talanta* 54 (2001) 531.
8. J. B. Noffsinger, N. D. Danielson, *Anal. Chem*. 59 (1987) 865.
9. X. Chen, M. Sato, *Anal. Sci*. 11 (1995) 749.
10. T. M. Downey, T. A. Nieman, *Anal. Chem*.64 (1992) 261.
11. Y. F. Zhuang, H. X. Ju, *Electroanalysis* 16: (2004) 1401.
12. J. H. Lin, H. X. Ju, *Biosens. Bioelectron*. 20 (2005) 1461.
13. H. Jiang, H. X. Ju, *Chem. Commun*. (2007) 404.
14. S. J. Guo, E. K. Wang, *Electrochem. Comm*. 9 (2007) 1252.
15. M. M. Richter, *Chem. Rev*. 104 (2004) 3003.
16. P. E. Michel, P. D. van der Wal, G. C. Fiaccabrino, N. F. de Rooij, M. Koudelka-Hep, *Electroanalysis*, 11 (1999) 1361.
17. D.Y. Tian, C.F. Duan, W. Wang, N. Li, H. Zhang, H. Cui, Y.Y. Lu, *Talanta*, 78 (2009) 399.
18. Y. Tao, Z. Lin, X. Chen, X. Wang, *Anal. Chim. Acta* 594 (2007) 169.
19. X. Zhang, A. J. Bard, *J. Phys. Chem*. 92 (1988) 5566.
20. C. J. Miller, P. McCord, A. J. Bard, *Langmuir* 7 (1991) 2781.
21. Y. S. Obeng, A. J. Bard, *Langmui*r 7 (1991) 195.
22. Y. Sato, K. Uosaki *J. Electroanal. Chem*. 384 (1995) 57.

23. I. Rubenstein, A. J. Bard, *J. Am. Chem. Soc*. 103 (1981) 5007.
24. L. B. Zhang, J. Li, Y. H. Xu, Y. H. Li, E. K. Wang, *Talanta* 79 (2009) 454.
25. H. Y. Wang, G. B. Xu, S. J. Dong, *Talanta* 55 (2001) 61.
26. A. N. Khramov, M. M. Collinson, *Anal. Chem*. 72 (2000) 2943
27. H. N. Choi, S. H. Cho, W. Y. Lee, *Anal. Chem*. 75 (2003) 4250.
28. H. Y. Wang, G. B. Xu, S. J. Dong, *Anal. Chim. Acta*, 480 (2000) 285.
29. M. Sykora, T. J. Meyer, *Chem. Mater*. 11 (1999) 1186.
30. M. M. Collinson, J. Taussig, S. A. Martin, *Chem. Mater*. 11 (1999) 2594.
31. Y. L. Li, H. Zhu, X. R. Yang, *Talanta* 80 (2009) 870.
32. F. R. Lei, Clay and clay minerals. China Geology: Beijing, 1992.
33. R. L. Frost, G. A. Cash, J. T. Kloprogge, *Vib. Spectrosc*. 16 (1998) 173.
34. J. H. Potgieter, S. S. Potgieter-Vermaak, P. D. Kalibantong, , *Miner. Eng*. 19 (2006) 463.
35. P. Ghosh, A. J. Bard, *J. Am. Chem. Soc*. 105 (1983) 5691.
36. Z. Navratilova, P. Kula, *Electroanalysis* 15 (2003) 837.
37. P. Innocenzi, H. Kozuka, T. Yoko, *J. Phys. Chem*. B 10 (1997) 2285.
38. E. Laviron, *J. Electroanal. Chem*. 101 (1979) 19.
39. G. B. Xu, L. Cheng, S. J. Dong, *Anal. Lett*. 32 (1999) 2311.
40. Z. H. Guo, Y. Shen, F. Zhao, M. K. Wang, S. J. Dong, *Analyst* 129 (2004) 657.
41. F. J. B. Noffsinger, N. D. Danielson, *Anal. Chem*. 59 (1987) 865.
42. W. Y. Lee, T. A. Nieman, *Anal. Chem*. 67 (1995) 1789.
43. J. K. Leland, M. J. Powell, *J. Electrochem. Soc*. 137 (1990) 3127.
44. F. Kanou, A. J. Bard, *J. Phys. Chem*. 103 (1999) 10469.